Hindawi
International Journal of Corrosion
Volume 2018, Article ID 4071352, 12 pages
https://doi.org/10.1155/2018/4071352

Research Article

Effect of Rare-Earth Elements on the Corrosion Resistance of Flux-Cored Arc-Welded Metal with 10CrNi3MoV Steel

Kai Wang,[1,2] **Qinghua Lu**,[1] **Zexin Jiang**,[3] **Yaoyong Yi**,[2] **Jianglong Yi**,[2] **Ben Niu**,[2] **Jinjun Ma**,[3] **and Huiping Hu**[1]

[1]*Foshan University, Foshan, China*
[2]*Guangdong Welding Institute (China-Ukraine E. O. Paton Institute of Welding), Guangzhou, China*
[3]*Guangzhou Shipyard International Co., Ltd, Guangzhou, China*

Correspondence should be addressed to Kai Wang; hfutwk927@gmail.com

Received 19 December 2017; Accepted 25 March 2018; Published 12 June 2018

Academic Editor: Flavio Deflorian

We modified the content of rare-earth elements (REE) in the flux-cored wire used to produce welds of high-strength low-alloy (HSLA) steel. The effect of REE addition on the microstructure as well as on the mechanical and electrochemical properties of the welded metal (WM) was investigated. REE-modified welded metals show very different responses during electrochemical impedance spectroscopy and the potentiodynamic polarization tests. The results indicate that the addition of REE of 0.3 wt.% facilitates a more uniform microstructure and improves both mechanical properties and corrosion resistance in welded metals.

1. Introduction

Welding is a common joining method, which is commercially used worldwide. The welding process for the manufacturing of a steel ship, for example, takes up 30%~40% of the overall production time. Flux-cored arc welding (FCAW) is a semiautomatic or automatic arc-welding process that involves the fusion of a flux-cored wire metal with a base metal. FCAW in particular is one of the most widely used welding techniques in the modern shipbuilding industry. The properties of FCAW joints are largely determined by the used welding consumables and the base metals used during the welding process.

10CrNi3MoV steel is a typical high-strength low-alloy steel (HSLA) that combines strength, toughness, and weldability thanks to Q-tempered processing. This type of steel is generally used as hull material in high-performance marine vehicles [1]. Due to the high-performance requirements of the welded joints in these vehicles, both low-temperature impact toughness and corrosion resistance of the welded metal determine the overall performance of 10CrNi3MoV steel.

One of the most effective approaches to improve toughness and corrosion resistance of a welded metal is to alter the welded metal composition by introducing alloying elements via the flux-cored wire to act as FCAW filler metals [2]. Generally, rare-earth elements (REE) are considered the most suitable microalloying elements for any mature alloy system. A minor addition of REE into the steel can significantly purify the liquid steel and modify any inclusions, which improves the steel properties [3–5]. The correct REE content can improve both impact toughness and temper brittleness of the welded components. This is due to its effect on grain refinement, grain boundary cleaning, and the suppression of grain boundary embrittlement [6]. Theoretical calculations show [7–9] that REE can increase the grain boundary cohesion in steel, which leads to toughening of the material via grain boundary segregation. Furthermore, the addition of REE can also enhance the high-temperature ductility of steel [10, 11]. Tomita [12] found that the addition of REE to vacuum-melted AF1410 steel can stabilize complex-inclusions and improve toughness. Gao et al. substantially improved the toughness of H13 steel by adding 0.015 wt.% REE, which favors finer and more dispersive inclusions [13]. The addition of REE to welded metals to SAW DH32 steel facilitates both inclusions and a small lattice disregistry, which improves elongation, tensile strength, and impact toughness of welded metals [14, 15]. It has also been reported that REE can improve the corrosion resistance of low-carbon steels [16, 17].

Table 1: Chemical composition of REE-Si-Fe (wt. %).

Ce	La	Nd	Pr	Sm	Ca	Si	Fe
12.56	4.43	1.41	0.55	4.53	3.1	40.9	Re

Table 2: Selected content of REE-Si-Fe for the weld samples in flux-cored wire (flux wt.%).

Weld Sample	REE-Si-Fe addition
REE0	-
REE1	0.3
REE2	0.5
REE3	0.7
REE4	1.0

However, the effects of REE on the features and properties of welded metal for 10CrNi3MoV steel, in particular, have received little attention, and no general agreement on the correct amount of REE in welded metal has been reported.

It is likely that REE elements can enhance the properties of welded metal through microstructural control during FCAW. In this work, the effect of REE addition to the flux-cored wire on both the microstructure and the properties of welded metal was investigated. In particular, we focused on the correlation between REE content and the resulting properties of the joints.

2. Experimental

The 10CrNi3MoV steel plates were arc-welded using flux-cored wires with different REE concentrations. REE (consisting of Ce-rich rare-earth ferrosilicon, REE-Si-Fe). The chemical composition of REE-Si-Fe is shown in Table 1. The flux-cored wires consist of a metal sheath and a powdered core; see Figure 1. They were prepared after the shaping of a cold-rolled strip and the filling of the hollow core with a powdered mixture and a XZ-YCX8 flux-cored wire production machine. In this study, the basic powdered core belongs to a rutile-fluorite alloying system with a filling ratio of 20%. The diameter of the finished wire was 1.2 mm. The chosen REE contents for the powdered cores are shown in Table 2. Five group samples with different REE concentrations in the welded metals were fabricated in the laboratory using identical welding conditions. The chemical composition and mechanical properties of the 10CrMo3NiV steel base metal are shown in Tables 3 and 4. The conditions and parameters for the FCAW process are listed in Table 5. The drawing of the FCAW grooves and welded metal samples for mechanical testing were prepared according to the Chinese standard GB/T17493-2008; see Figure 2.

The chemical composition of the welded metals (except for carbon, C) was determined using a JY ULTIMA inductive coupled plasma emission spectrometer. The C content was determined using a LECO CS600 carbon-sulphur spectrometer. The phases within welded metals were identified with a D/max-IIIA X-ray diffractometer (XRD). Each welded metal sample was observed and analyzed with a DMM-440D optical microscope (OM) and a JEOLJXA-8100 scanning electron

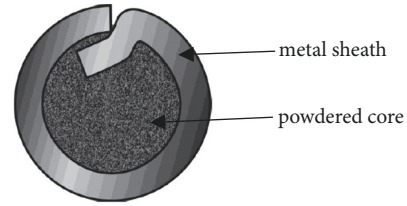

Figure 1: Schematic of a flux-cored wire.

microscope (SEM) and its accessory EDX (OXFORD-7412) after grinding, polishing and etching with a 4% natal solution. The microhardness of the welded metal was measured using a HVS-1000 micro Vickers hardness tester with a load of 0.3 kgf, using four points on the same circumference of the 1/2 radius for each sample. Samples for electrochemical impedance spectroscopy (EIS) and potentiodynamic polarization (PP) testing were taken from the center of the welded metals along the longitudinal direction. This was done via linear cutting into squares of 10 mm×10 mm×0.5 mm. Before the electrochemical tests, the samples were polished with 2000-grid sandpaper, degreased with acetone, washed with distilled water, and blow-dried. The working areas of the tested samples were 1cm^2, and the remaining areas of the samples were sealed with wax. The EIS and PP tests were carried out using an Ametek P4000 electrochemical workstation with a three-electrode system. The working electrode was the tested sample (1 cm^2 working area), the auxiliary electrode was a Pt plate, and the reference electrode was saturated calomel electrode (SCE). The electrolyte was a 3.5 wt.% NaCl water solution. The working electrode was soaked in the electrolyte in open-circuit-potential (OCP) mode for 30 min before testing. The EIS mode was set as a frequency of 10^{-2} Hz ~ 10^5 Hz versus OCP with an AC drive signal amplitude of ±5 mV. The following potentiodynamic polarization mode was chosen for a scanning potential range of -1.0 V ~ +1.5 V versus OCP with a scanning speed of 1 mV/s. The polarized samples were observed with a SEM.

3. Results and Discussion

3.1. Chemical Composition Analysis. The chemical compositions of the welded metals (only key elements) are listed in Table 6. The REE addition causes significant changes of the C and Ni content but only with slight variations in the Si, Mn, and Mo content of the welded metals. Furthermore, there are rare changes in the Al and Ti content of the welded metals.

3.2. Mechanical Properties of the Welded Metals. Table 7 and Figure 3 show the mechanical properties of the FCAW-welded metals with different REE added. In Figure 3(a), the values for tensile strength, yield strength, and elongation ratio increase suddenly after the REE addition of 0.3%. The above test results, however, indicate a gradual decrease when the REE content exceeds 0.3%, which is lower than for the REE-free welded metal (REE0) before the REE addition of 1.0%. Figure 3(b) shows the low-temperature impact energy for the welded metals. The impact energy for all welded metals with added REE is higher than for REE-free welded metals,

Table 3: Chemical composition of 10CrNi3MoV steel (wt. %).

C	Si	Mn	Ni	Mo	Cr	V	P	S
0.11	0.31	0.39	2.72	0.23	1.05	0.08	0.010	0.005

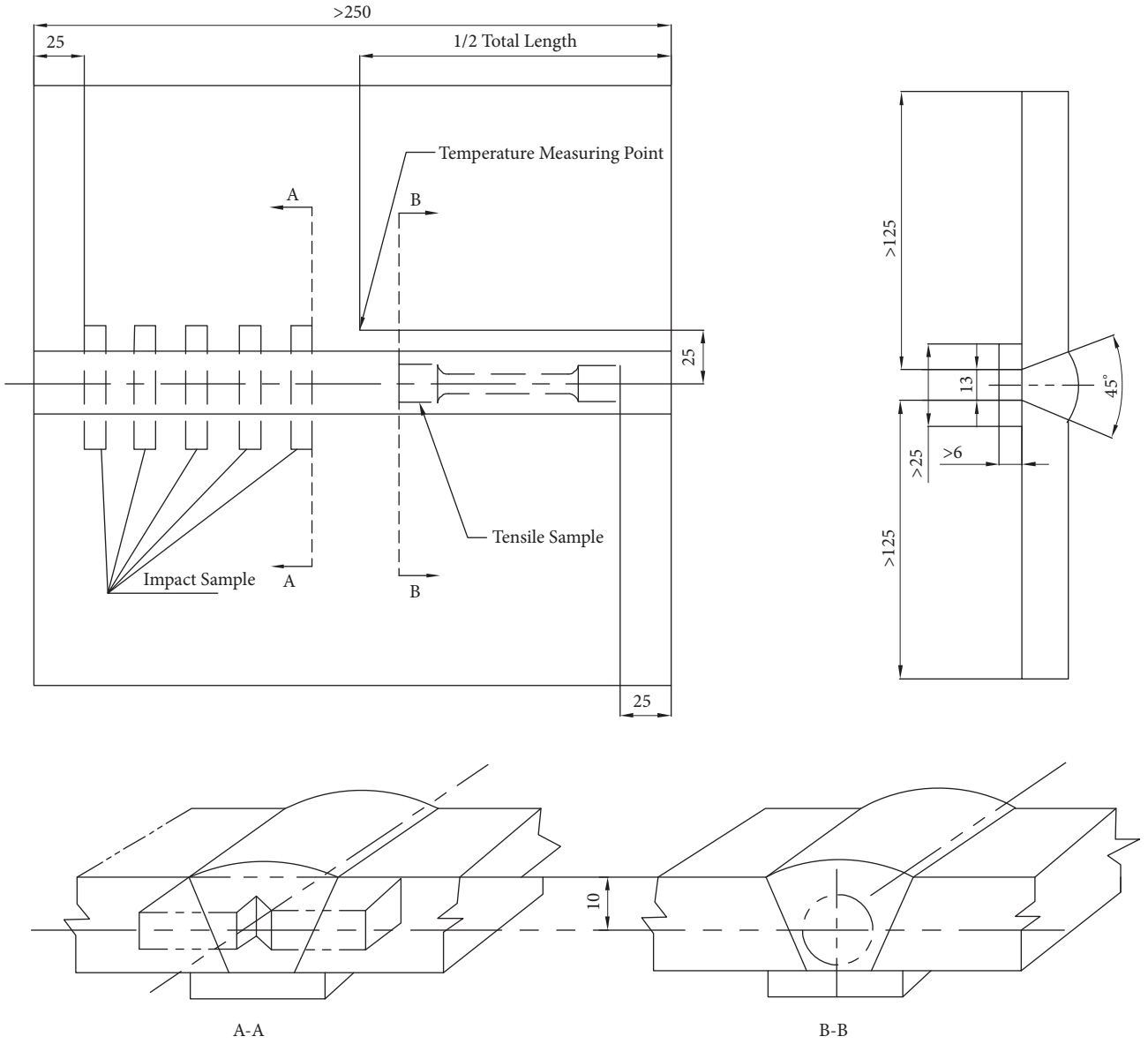

Figure 2: Schematic illustrating the grooves in the samples (mm).

Table 4: Mechanical properties of 10CrNi3MoV steel.

Yield Strength/MPa	Tensile Strength/MPa	Elongation/%	A_k -20°C/J
590~745	670~850	≥16	≥80

and it increases significantly as the REE content increases to 0.3%. However, the impact energy of the welded metals causes a slight decrease followed by a further REE content increase to 1.0%. The microhardness of the relevant samples is very low. The slight fluctuation may be due to the presence of C in the welded metals [18]. This is because a higher C content in the REE1 and REE2 welded metals was detected; see Table 6. In other words, adding REE improves indeed the mechanical properties of the welded metals significantly. The correct addition of the right amount of REE can improve the strength of the welded metals, while REE adding over 0.7% reduces the strength.

3.3. Microstructural Analysis. Figure 4 shows the optical morphologies of the FCAW-welded metals with different REE additions. It is hard to identify any prior austenite

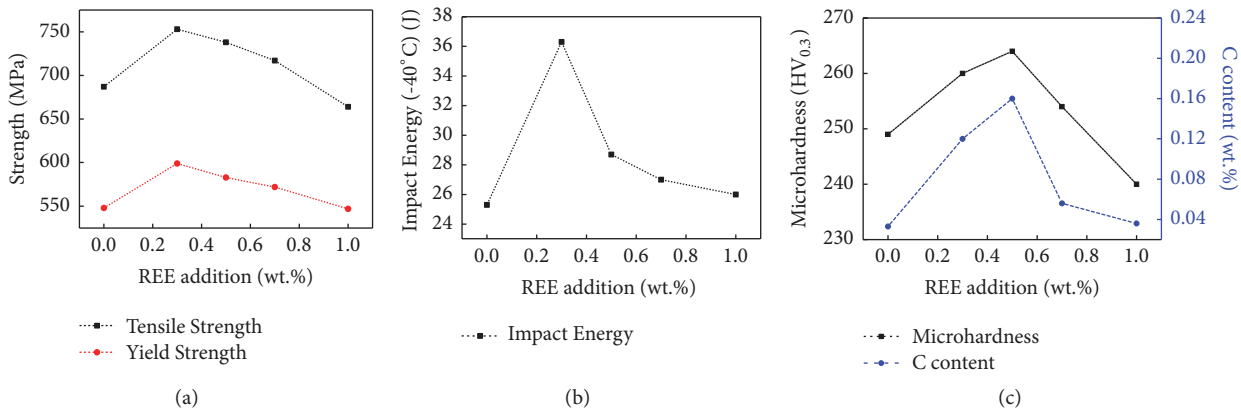

Figure 3: Mechanical properties of FCAW-welded metals for different REE contents: (a) tensile properties; (b) low-temperature impact toughness; and (c) microhardness.

Table 5: Welding parameters for FCAW.

Plate form and dimensions (mm)	Flat, 300 ×150 ×14
Welding Machine	EWM
Power Mode	DCEP
Electrode	As-prepared wires
Protective gas	M21 (80% Ar + 20% CO_2)
Gas flow rate (L/min)	17 ~ 20
Preheating temperature (°C)	150
Current (A)	240
Voltage (V)	26
Interpass temperature (°C)	150 ~ 180
Welding speed (mm/s)	6.3 ~ 7.9
Cooling after welding	Air

grain boundaries (PAGB), which means a complete phase transformation (to ferrite) occurred during cooling. The microstructure of REE-free welded metal consists of proeutectoid ferrites (PF), acicular ferrites (AF), and a small amount of bainites (B); see Figure 4(a). No bainite was formed in the welded metals with REE added; see Figures 4(b)–4(e). This indicates that a microstructure of different forms of ferrites, i.e., AF, lath ferrites (LF), and granular ferrite (GF), was formed. After REE addition of 0.3% and 0.5%, as shown in Figures 3(b) and 3(c), the microstructure of the welded metals becomes more refined. In addition, the PF size is limited due to inhibited nucleation of PF. Furthermore, there is increased nucleation and AF growth due to the added REE. Some small LF formed due to the continuous growth of AF. The total amount of grain boundaries increases clearly because of the formation of AF. There is a high density of dislocations in the interior of the acicular ferrites, with few low-angle boundaries. These require higher energy for the microcracks to cross the AF, which improves crack growth-resistance [19]. Because there are many large-angle grain boundaries among adjacent grains, which can increase the resistance of dislocation motion and the plastic deformation, the formation of AF increases both strength and low-temperature impact toughness [20, 21]; see Figure 3. When the REE content REE exceeds 0.5%, the inhibiting property of PF nucleation is restored. This is a result of the pollution of the grain boundaries by REE, which appears as disproportionate growth of PF [22]; see Figures 4(d) and 4(e). The REE addition of 0.3% and 0.5% can refine the grains by promoting the formation of AF effectively. This improves the mechanical properties of welded metals. When the REE content exceeds 0.5%, AF is limited with its growth promotion of LF and PF. This leads to a reduction in strength and low-temperature affects the toughness of the welded metals.

If second-phase particles are of suitable size with a uniform distribution, they could act as nuclei during the solidification process. Studies [23, 24] show that particles finer than 0.6 μm facilitate the nucleation of ferrite, while even more effective nucleation occurs in the 0.2~0.6 μm range. Figure 5 shows the SEM images of the welded metals with different amounts of REE added. The number of second-phase particles in the REE-free welded metal is small, and their size is relatively large (up to 3.3 μm in diameter); see the dark spots in Figure 5(a). It is clear that the number of second-phase particles increases significantly, while the average size decreases gradually REE for higher REE content; see Figures 5(b)–5(e). This is substantially different from the REE-free welded metal, based on the measurement of more than 100 particles. Following a further increase of the REE content (up to 1.00%), the number of second-phase particles continues to increase with a discrete distribution and reduced average size. Some second-phase particles (on a microscale) are beginning to appear in the field of view.

Both the number of second-phase particles and the fraction of different grain sizes were counted using the SEM images. The statistical results are shown in Figure 6. For a higher REE content, the size range for the second-phase particles becomes gradually smaller. Some oversized particles (up to 3.3 μm in the REE-free welded metal) do not appear in the REE-added welded metals. The fractions of second-phase particles between 0.2 and 0.6 μm in Figures 6(a)–6(e) are 70.2%, 77.8%, 74.4%, 49.9%, and 46.4%, respectively. This shows the first increasing and then decreasing trend if the REE content increases. However, the fractions of particles

Table 6: Chemical composition of the welded metals (wt. %).

welded metal sample	C	Si	Mn	Mo	Al	Ti	Ni
REE0	0.033	0.30	1.59	0.23	0.013	0.030	2.39
REE1	0.12	0.25	0.97	0.11	0.011	0.028	1.07
REE2	0.16	0.29	1.44	0.17	0.014	0.031	1.77
REE3	0.056	0.42	1.47	0.23	0.014	0.029	2.41
REE4	0.036	0.33	1.42	0.25	0.013	0.032	2.34

Table 7: Mechanical properties of the welded metals with different amounts of REE.

welded metal	Tensile Strength/MPa	Yield Strength/MPa	Elongation /%	Average Impact Energy at -40°C/J	Micro-hardness/$HV_{0.3}$
REE0	687	548	21.2	25.3	249
REE1	753	599	22.5	36.3	260
REE2	738	583	20	27.7	264
REE3	717	572	14.2	27	254
REE4	664	547	14.5	28	240

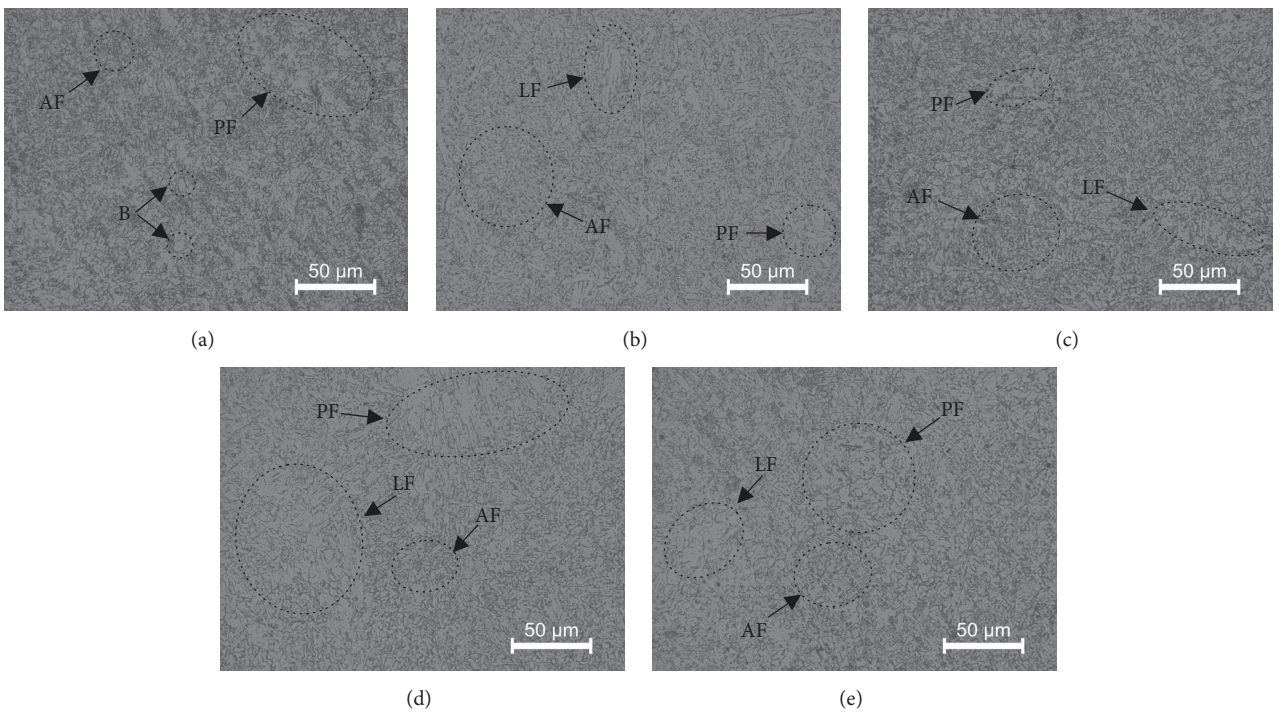

Figure 4: OM images of FCAW-welded metals for different REE contents:(a) REE-free, (b) 0.3 wt.%, (c) 0.5 wt.%, (d) 0.7 wt.%, and (e) 1.0 wt.%.

below 0.2 μm are 0%, 0%, 8.1%, 28.1%, and 44.9%, respectively, which represents an upward trend for increasing REE content. Hence, a very high REE content can reduce the size of the second-phase particles, and the slope describing the mechanical properties of welded metals becomes negative. When the REE content is optimal (0.3%), most of the second-phase particles form in the size range of 0.2 to 0.6 μm, which facilitates the formation of AF and results in the best mechanical performance of welded metals.

The EDS results for the second-phase particles are shown in Table 8. There are mainly three elements (Fe, Mn, and Ni) in the matrix, with a fluctuating variation of the components. However, the types and compositions of the elements in the particles of different samples are somewhat different, whose main elements consisted of O, Al, Si, Ti, Mn, and Fe. Because the particles are located within the matrix, the EDS determination will include part component of the matrix into the results. Moreover, the content of Fe is about 45%, the highest of all elements; it can be considered that the Fe mainly stems from the matrix. There is a small amount of S in the second-phase particles in three groups of samples with 0.3% REE, 0.5% REE, and 0.7% REE, respectively. A certain amount of S element in the alloy steel is beneficial to the improvement of its machinability. However, for the welded

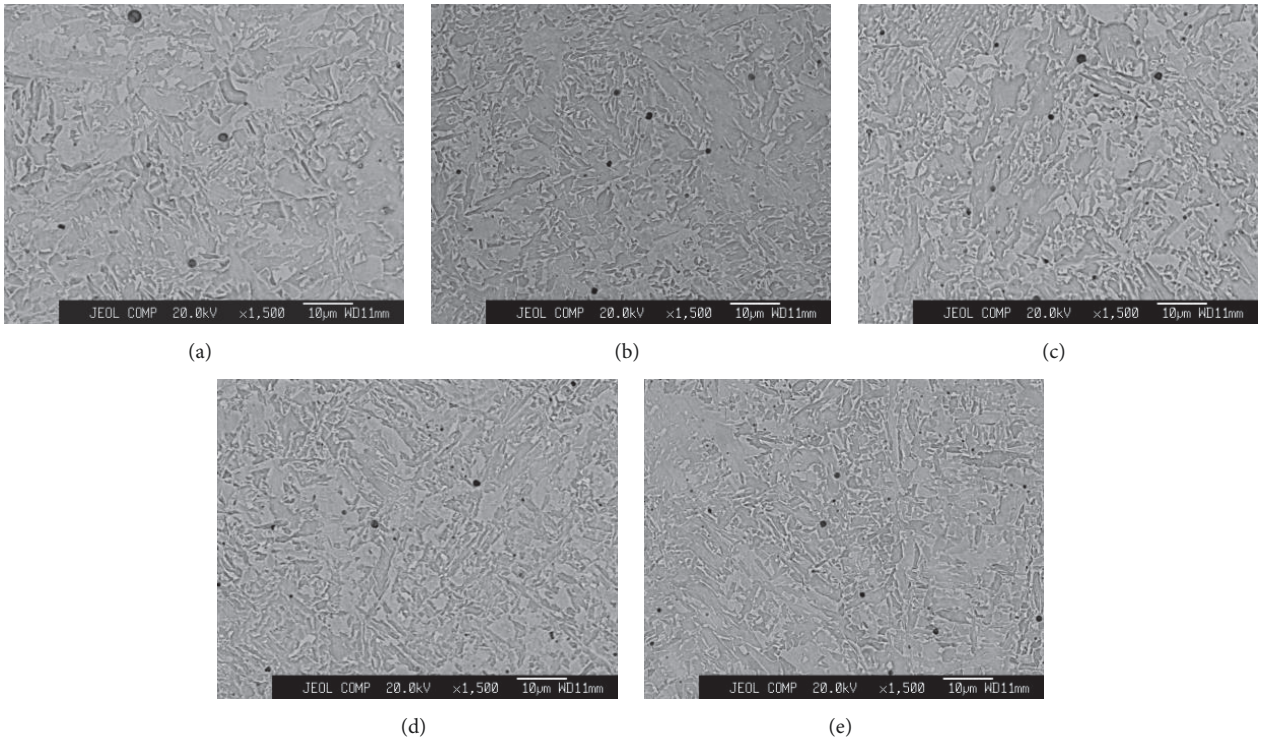

Figure 5: Typical SEM images of welded metals with different REE contents: (a) REE-free, (b) 0.3 wt.%, (c) 0.5 wt.%, (d) 0.7 wt.%, and (e) 1.0 wt.%.

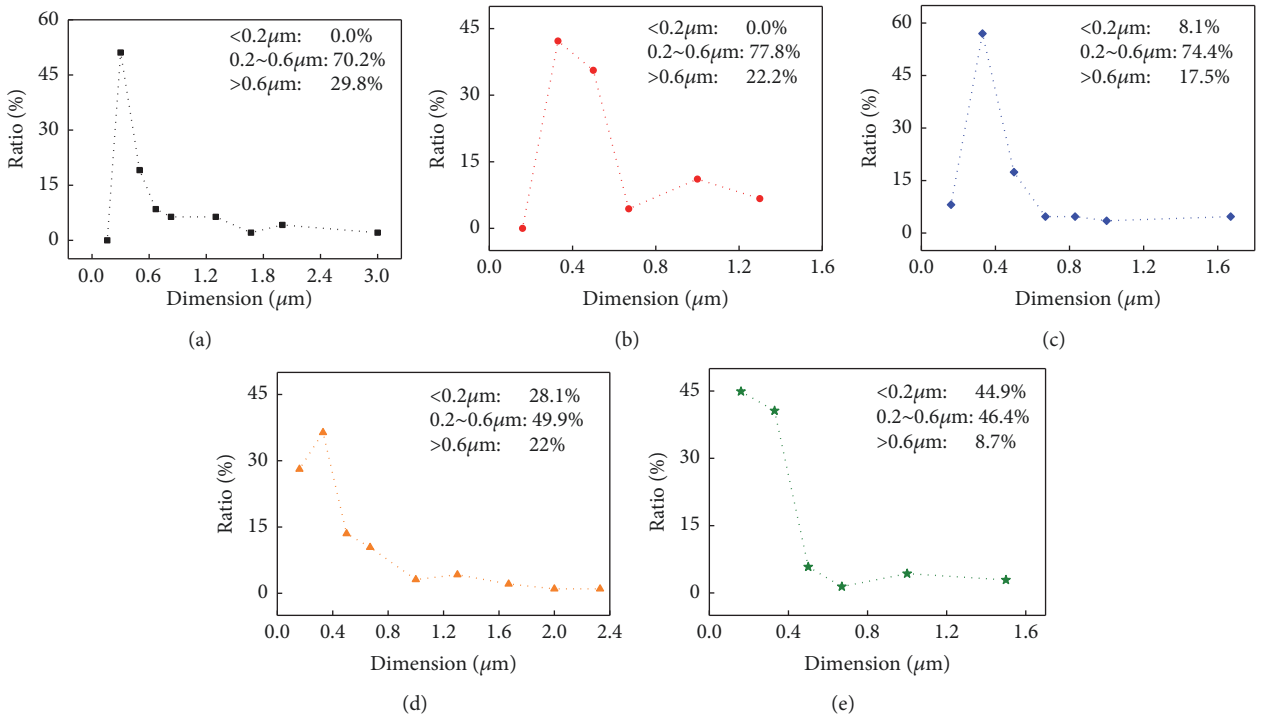

Figure 6: Dimension (size) and ratio of the second-phase particles in welded metals with different REE contents: (a) REE-free, (b) 0.3 wt.%, (c) 0.5 wt.%, (d) 0.7 wt.%, and (e) 1.0 wt.%.

Table 8: EDS results of the matrix or second-phase particles for each welded metal with varying REE content.

Items	Matrix					Second-phase particle					
Elements	Mn/%	Fe/%	Ni/%	O/%	Al/%	Si/%	Ti/%	Mn/%	Fe/%	S/%	Ni/%
REE0	1.42	96.27	2.31	16.86	4.26	2.57	14.12	18.55	42.91	/	0.73
REE1	1.72	96.13	2.15	16.92	3.91	6.47	6.73	15.34	49.85	0.14	/
REE2	2.39	94.99	2.62	14.38	5.25	5.10	9.29	17.32	46.65	2.01	/
REE3	1.43	95.61	2.96	20.61	6.09	6.00	12.25	13.30	39.25	2.50	/
REE4	1.23	96.39	2.38	16.68	4.53	6.66	6.48	14.99	50.67	/	/

metal, a tiny amount of S can greatly reduce its performance. In this work, it can be found that correct REE content can aid S to accumulate into the second-phase particles, which originally dissolved in the matrix. Thus, it will reduce the harmful effects on the matrix to increase the strength of weld metal. This conclusion is consistent with the above discussion of the mechanical properties in Figure 2. With the increasing REE addition, the relative contents of the nonmetallic elements O, Si, and S in the second-phase particles show a rising trend, and the content of Al and Fe increased slightly, while Ti and Mn decreased slightly. Mn and Ti tend to deoxidize and remove impurities to form refractory-phase impurities like MnS or TiO, combined with S or O. These discharged from the welded metal into the welding slag with the right content of nonmetallic elements O and S. Enrichment with oxygen in the welded metal tends to increase the possibility of the generation of weld blowholes, which can induce cracks and become the sources of microcracks under external load. This decreases both the strength and the low-temperature impact toughness of the weld metal. Sulphur could form banded FeS, when combined with Fe and weaken the consistency of the weld metal. The right amount of Si cannot only act as a deoxidant but also form Al-Mn silicate particles and facilitate nucleation. Therefore, adding REE causes the elements of O, S, and Si to accumulate in the second-phase particles instead of the matrix, which purifies the matrix and refines the grains or microstructure effectively. As a result, the strength and low-temperature impact toughness of the weld metal are improved using REE.

Phase compositions for each sample were determined using XRD, and the results are shown in Figure 7. The matrix consists of α-Fe (AF), and the second phase consists mainly of an Al-Ti phase and $(Al, Mn)_xSiO_4$ (Al-Mn silicate) phase. Furthermore, $(Al, Mn)_xSiO_4$ is composed of a variety of metallic or nonmetallic oxides including Al_2O_3, MnO, and SiO_2, which play a strong role in deoxygenation and greatly reduce oxygen in the welded metals. During the solidification process of the weld pool, the second-phase particles, which consist of Al_2O_3, MnO, and SiO_2, formed preferably with high surface-energy [25], where the crystal nuclei for ferrite form. In this way it can substantially reduce the potential barrier for nucleation during the phase transformation from γ to α phase. The second-phase particles in the weld metal are mostly a complex mixture of different phases. Therefore, each phase can be regarded as a high-energy region and form a nucleus for acicular ferrite. Multidimensional nucleation occurs at the end and causes acicular ferrite to overlap, which results in refined grains.

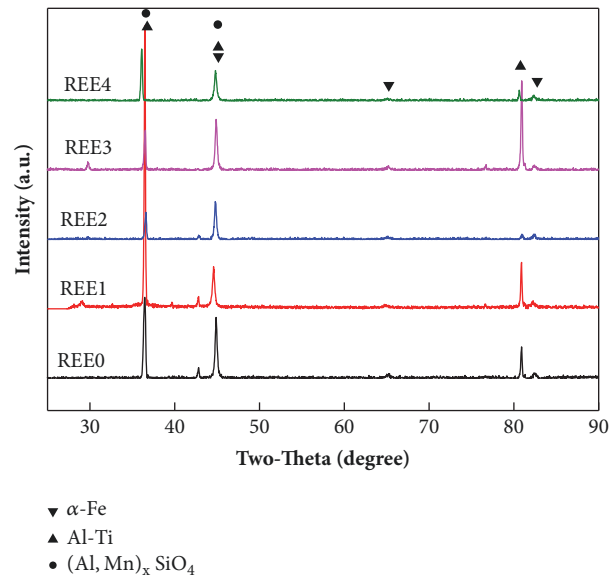

Figure 7: XRD analysis results of different FCAW-welded metals.

3.4. Electrochemical Properties. The EIS responses of the FCAW-welded metals with different REE contents in a 3.5 wt.% NaCl solution were measured to study effects on the electrochemical properties. Our results are shown as Nyquist, Bode, and Bode-phase plots in Figure 8. The Nyquist plots of all welded metals are imperfect semicircles (Figure 8(a)), i.e., capacitive arcs with similar capacitive response. Only a single depressed semicircle for each welded metal appears in the Nyquist plots, which indicates that only one time-constant is present in EIS. The imperfect semicircle-diameter for REE4 is the largest. It shows the largest capacitive arc and the best antidissolution properties. The imperfect semicircle-diameters for REE welded metals, with REE added (REE1, REE2 and REE3), are smaller than the REE-free welded metal. In the low-frequency range of the Bode plots (Figure 8(b)), the samples with higher electrical resistance possess stronger corrosion resistance. This is consistent with our analysis of the above Nyquist plots. In Figure 8(c), each spectrum shows one single sharp peak, with maximum phase-angles below 70°. This means the EIS capacitive response of the welded metals, with or without REE addition, is not pure or ideal. Hence, there is only one time-constant and low reactive resistance, which is similar to the results reported by R.M. Domene et al. [26].

To simulate the measured impedance data and explain the general corrosion process, the equivalent circuit shown

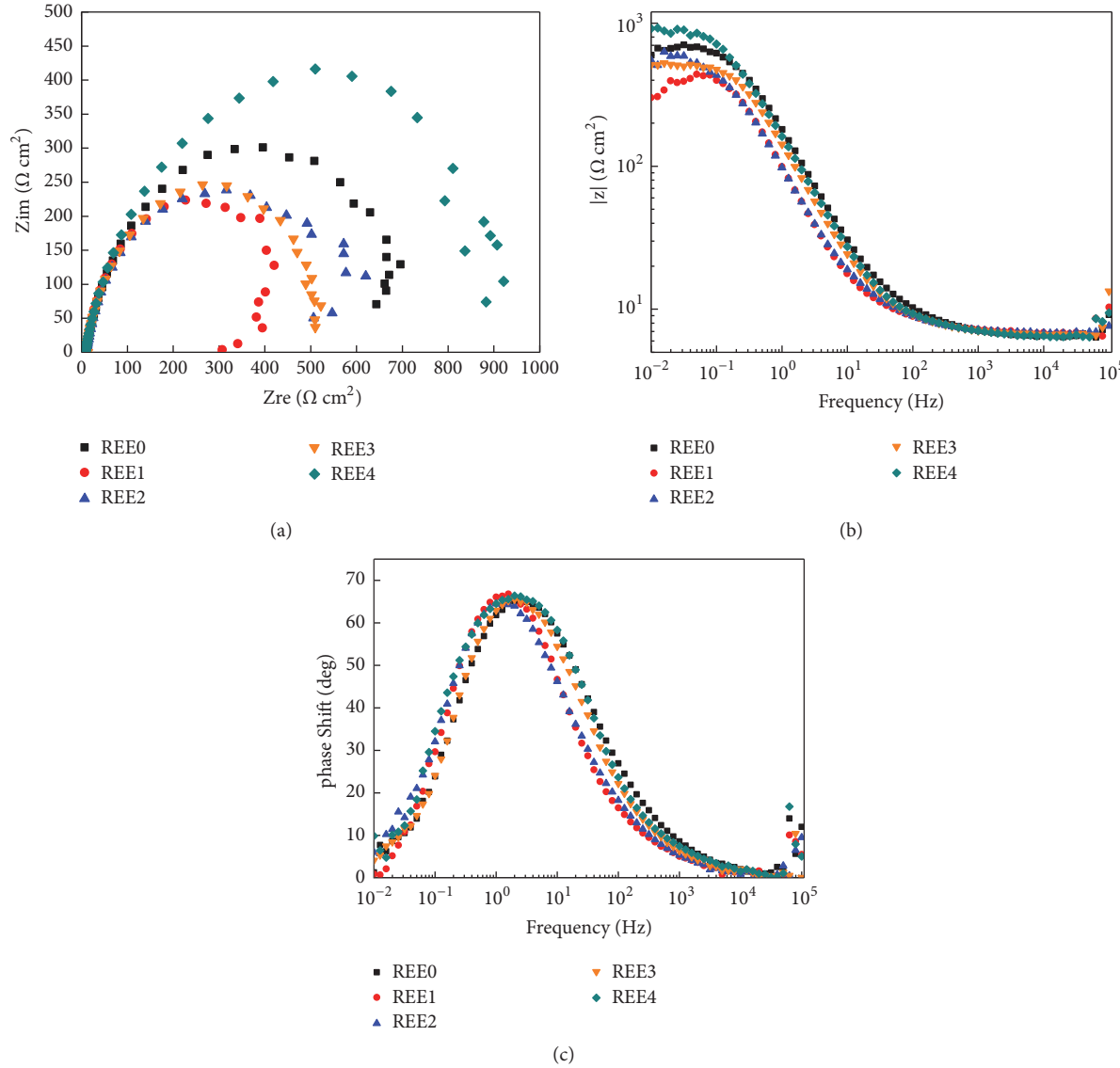

Figure 8: (a) Nyquist, (b) Bode, and (c) Bode-phase plots for the FCAW-welded metals with different REE contents versus OCP in a 3.5wt% NaCl solution.

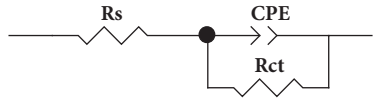

Figure 9: Equivalent circuit used to model the experimental EIS data.

in Figure 9 was adopted. The variations of the impedance parameters are shown in Table 9, and the respective errors are below 5%. Consistent with the active dissolution mechanism, R_s is the solution resistance, and R_{ct} represents the charge-transfer resistance from the metal to the electrolyte, which can be defined as the corrosion resistance for the sample in the electrolyte. Furthermore, C_{PE} accounts for the constant phase element corresponding to the metal in this equivalent model, as reported by Y. Chen et al. [27]. The welded metal

Table 9: Impedance parameters for the EIS-tested welded metals.

welded metals	R_s ($\Omega \cdot cm^2$)	Capacitance (F)	R_{ct} ($\Omega \cdot cm^2$)
REE0	8.03	0.0006136	637.3
REE1	8.17	0.001366	401.7
REE2	8.19	0.001321	529.7
REE3	8.13	0.0008468	493.8
REE4	7.89	0.000742	843.7

(with 1.00 wt.% REE addition) has the highest R_{ct} (983.0 $\Omega \cdot cm^2$), and the REE1 welded metal has the lowest R_{ct} (447.6 $\Omega \cdot cm^2$). Only the REE4 welded metal with 1.00 wt.% REE content shows a higher R_{ct} than its counterpart for the REE-free welded metal.

Table 10: Electrochemical data of the welded metals with different REE contents as obtained from potentiodynamic polarization measurements in 3.5 wt.% NaCl solution.

welded metals	E_{corr} (mV)	I_{corr} (μA/cm^2)	R_p (Ohms/cm^2)
REE0	-344	24.9	1047.2
REE1	-546	13.4	1945.7
REE2	-544	14.0	1862.5
REE3	-403	13.6	1918.3
REE4	-527	16.5	1579.5

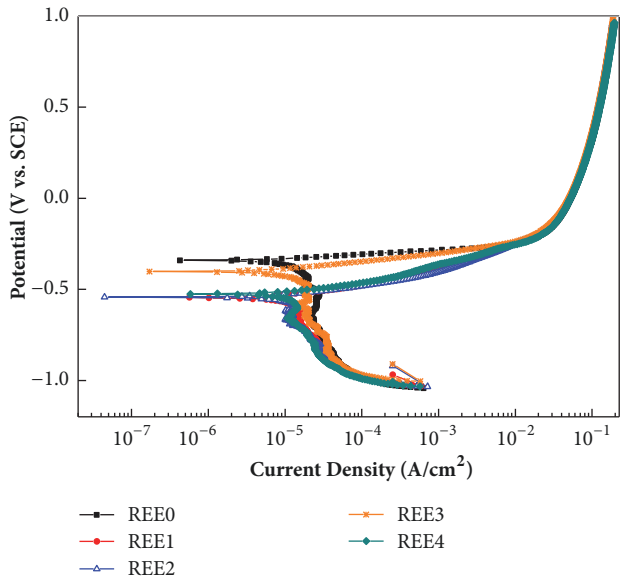

Figure 10: Potentiodynamic polarization curves for the welded metals with different REE contents.

After the EIS tests, potentiodynamic polarization measurements were carried out, in a 3.5 wt.% NaCl solution at room temperature. The results are shown in Figure 10 and Table 10. Corrosion potential (E_{corr}) is a static indicator for electrochemical corrosion resistance to describe corrosive susceptibility of a material. In this study, all welded metals with REE show a lower corrosion potential than the REE-free welded metal; see Table 10. The REE-free welded metal has the highest E_{corr} (-344 mV), while the REE1 with the minimum REE addition has the lowest E_{corr} (-546 mV). This indicates a small REE addition has already a significant effect on the corrosive susceptibility in welded metals. However, higher corrosive susceptibility does not mean the material corrodes easily. According to the Tafel rule, corrosion current density (I_{corr}) is a key factor and closely related to the corrosion-dissolution rate. Furthermore, the related polarization resistance (R_p) is used to determine the corrosion rate at any given time. In addition, lower I_{corr} and higher R_p indicate a higher corrosion resistance. The polarization curves for all welded metals with or without REE show typical signs of active dissolution in the 3.5 wt.% NaCl solution. The active dissolution mechanism is further confirmed by the high I_{corr} compared to the calculated 10 μA/cm^2 for all welded metals; see Table 10. REE-free welded metal (REE0) has the highest I_{corr} (24.9 μA/cm^2) and the lowest R_p (1047.2 Ohms/cm^2). REE could retard the anodic process and cathode process to reduce the corrosion rate of welded metal. E_{corr} negatively moved, due to greater effect of REE on the equilibrium potential of cathode reaction [28]. The shapes of all polarization curves are basically the same, which shows that the corrosion mechanism of different REE has not changed. Both I_{corr} and R_p of the welded metals improved, due to the addition of REE. They are better than for Re-free welded metal. The REE addition could reduce the corrosion-dissolution rate and improve corrosion resistance of welded metals. REE1, with an REE addition of 0.2%, shows the strongest corrosion reduction effect, for the highest R_p (1945.7 Ohms/cm^2) and the lowest I_{corr} (13.4 μA/cm^2). In other words, the reduction effect weakens after adding REE, due to the increased I_{corr} and reduced R_p for REE2 to REE4.

It is interesting that R_{ct} and R_p of the welded metals with different REE contents show different trends. Considering the effect of REE, the difference between the R_{ct} and R_p values might depend on the second-phase particles. The correlations between second-phase particle size and the resistances are shown in Figure 11. It has been reported that a ferrite phase dissolves better during galvanic corrosion [29], and secondary phases act as a pathway in a corrosive environment [30]. The REE second-phase particles have no significant effect on the resistance of REE-free welded metals. REE R_{CT} changes inversely with the size of the second-phase particles in welded metals that contain REE; see Figures 11(b) and 11(d). The second-phase particles provide charge-transfer channels during the EIS tests. Large second-phase particles provide larger channels, which increase the active dissolution efficiency. By increasing the content of REE, the refining particles restrict the charge-transfer process between the welded metal and the electrolyte. This increases R_{ct} and leads to better corrosive resistance. The polarization test considers complex factors for the evaluation of corrosion properties, including the EIS response. For REE-containing welded metals, the R_p values are proportional to the second-phase particle sizes of the welded metals; see Figures 11(a) and 11(c). The R_p values are the opposite of the R_{ct} values. Welded metals with larger second-phase particles show higher R_p values. This can be due to the electric-potential increase of the second-phase particles containing REE. The REE content affects both sizes and ratios of the second-phase particles and the corrosion properties of HSLA welded metals as well as the mechanical properties.

The morphology of the welded metals after electrochemical testing is shown in Figure 12. Significant microcracks can be observed on the corrosive surface of the REE-free welded metal shown in Figure 12(a). The number of microcracks varies with the R_p values of the different REE-containing welded metals. No obvious microcracks were found on the corrosive surface of the REE1 sample; see Figure 12(b).

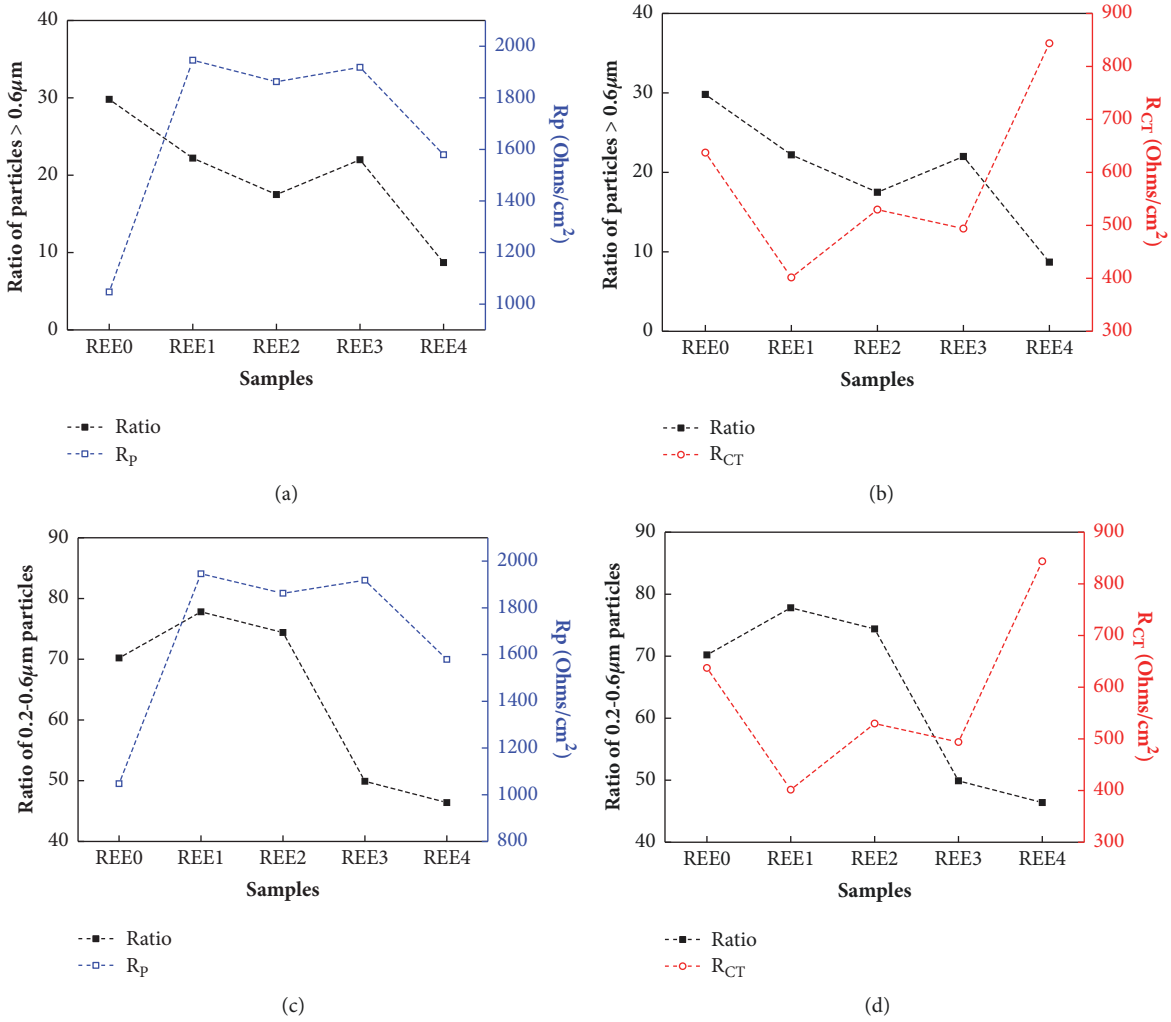

Figure 11: Correlation between second-phase particle sizes and the resistance in different welded metals.

However, microcracks REE can be seen clearly on the REE4 sample in Figure 12(e). During the electrochemical tests, the microcracks generated in the oxide films provide the channels for the electrolytes to infiltrate the oxide films. As a result, the charge-transfer process from the welded metal to the electrolyte accelerated. Both the REE-modified second-phase particles and microstructure of the welded metal facilitate the formation of dense oxide films thanks to the addition of REE.

For 10CrMo3NiV high-strength steel, the corrosion stability and the microstructure of the welded metal were significantly affected by the addition of REE, from the perspective of the effect on the size and ratio of second-phase particles. The result of the EIS tests and the potentiodynamic polarization curves indicates that the added REE in the flux-cored wire improves corrosion resistance in 10CrMo3NiV welded metals. To obtain detailed results of the second-phase particles affecting the electrochemical behavior of the welded metals, we plan to use scanning vibrating electrode technology (SVET) in further study. This will help reveal the underlying mechanism of REE: how REE change for different corrosive times and electrolytes.

4. Conclusions

Rare-earth elements were added to the flux-cored wire to modify the performance of FCAW-welded metals with 10CrMo3NiV steel. Both OM and SEM studies indicate that the REE content changes the microstructure of welded metals by refining the second-phase particles. A content of 0.3 wt.% REE in the flux-cored wire is optimal to facilitate suitable second-phase particles in both the welded metal (0.2 μm to 0.6μm in diameter) and the main acicular ferrite microstructure. This amount of REE also helps avoid the accumulation of nonmetallic elements and improves the mechanical properties of the welded metals. Both potentiodynamic polarization and EIS tests show that REE addition reduces the charge-transfer channel effect of the second-phase particles. Overall, the corrosion properties as well as the mechanical properties of a welded metal can be improved substantially by adding 0.3 wt.% REE.

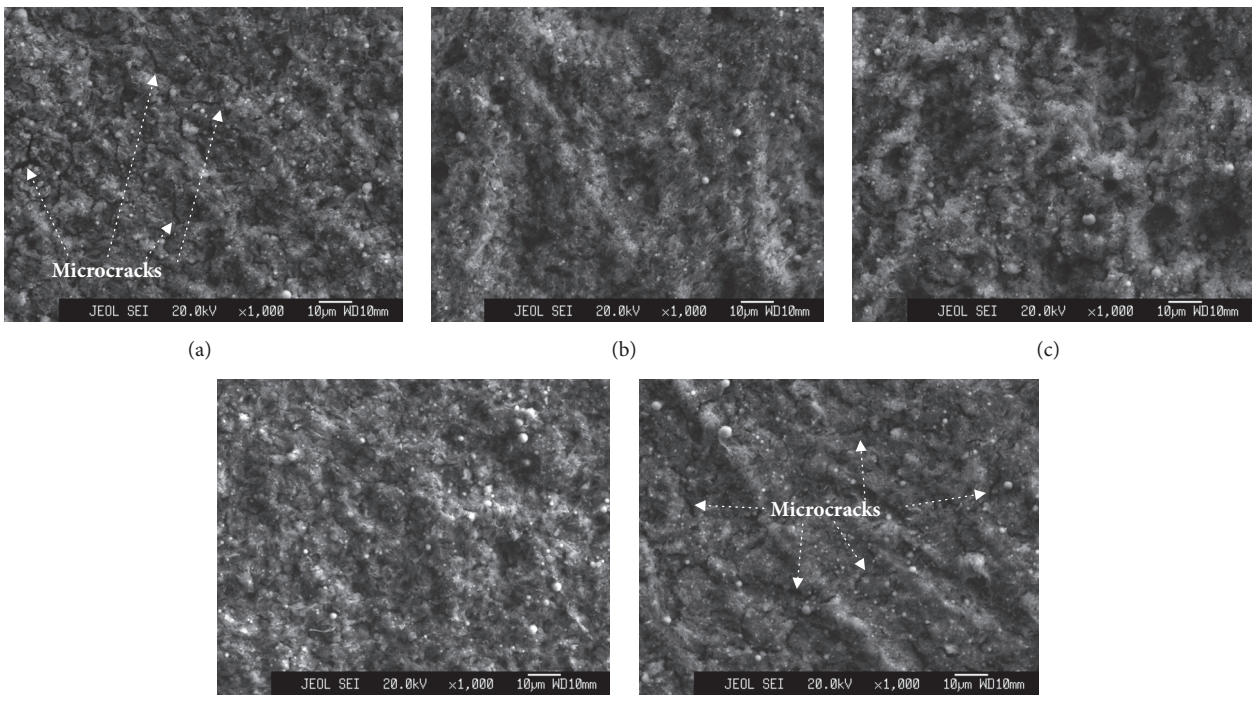

Figure 12: Morphology of the welded metals with different REE contents: (a) REE-free, (b) 0.3 wt.%, (c) 0.5 wt.%, (d) 0.7 wt.%, and (e) 1.0 wt.%, after electrochemical testing.

Conflicts of Interest

The authors declare that they have no conflicts of interest.

Acknowledgments

This research was supported by the National Natural Science Foundation of China (no. 51601043), the Scientific Program of GDAS (2016GDASPT-0205), the Technical Project of Guangdong and Guangzhou (201604046026, 2016B090918120, 201508030024, and 201704030112).

References

[1] *Committee on Effective Utilization of Weld Metal Yield Strength, Effective Use of Weld Metal Yield Strength for HY Steels*, National Materials Advisory Board, Washington DC, Wash, USA, 1983.

[2] J. H. Kim, J. S. Seo, H. J. Kim, H. S. Ryoo, K. H. Kim, and M. Y. Huh, "Effect of weld metal microstructures on cold crack susceptibility of FCAW weld metal," *Metals and Materials International*, vol. 14, no. 2, pp. 239–245, 2008.

[3] Y.-W. Xu, S.-H. Song, and J.-W. Wang, "Effect of rare earth cerium on the creep properties of modified 9Cr-1Mo heat-resistant steel," *Materials Letters*, vol. 161, pp. 616–619, 2015.

[4] J. Hufenbach, A. Helth, M.-H. Lee et al., "Effect of cerium addition on microstructure and mechanical properties of high-strength Fe85Cr4Mo8V2C1 cast steel," *Materials Science and Engineering: A Structural Materials: Properties, Microstructure and Processing*, vol. 674, pp. 366–374, 2016.

[5] W. M. Garrison Jr. and J. L. Maloney, "Lanthanum additions and the toughness of ultra-high strength steels and the determination of appropriate lanthanum additions," *Materials Science and Engineering: A Structural Materials: Properties, Microstructure and Processing*, vol. 403, no. 1-2, pp. 299–310, 2005.

[6] H.-L. Liu, C.-J. Liu, and M.-F. Jiang, "Effect of rare earths on impact toughness of a low-carbon steel," *Materials and Corrosion*, vol. 33, no. 1, pp. 306–312, 2012.

[7] G. Liu, G. Zhang, and R. Li, "Electronic theoretical study of the interaction between rare earth elements and impurities at grain boundaries in steel," *Journal of Rare Earths*, vol. 21, no. 3, pp. 372–374, 2003.

[8] D. Zhang, C. Wu, and R. Yang, "Interaction between cerium and phosphorus segregating in the grain boundaries in α-Fe studied by computer modelling and Auger electron spectroscopy," *Materials Science and Engineering: A Structural Materials: Properties, Microstructure and Processing*, vol. 131, no. 1, pp. 93–97, 1991.

[9] S. Song, H. Sun, and M. Wang, "Effect of rare earth cerium on brittleness of simulated welding heat-affected zones in a reactor pressure vessel steel," *Journal of Rare Earths*, vol. 33, no. 11, pp. 1204–1211, 2015.

[10] X. Jiang and S.-H. Song, "Enhanced hot ductility of a Cr-Mo low alloy steel by rare earth cerium," *Materials Science and Engineering: A Structural Materials: Properties, Microstructure and Processing*, vol. 613, pp. 171–177, 2014.

[11] L. Chen, X. Ma, M. Jin, J. Wang, H. Long, and T. Mao, "Beneficial Effect of Microalloyed Rare Earth on S Segregation in High-Purity Duplex Stainless Steel," *Metallurgical and Materials Transactions A: Physical Metallurgy and Materials Science*, vol. 47, no. 1, pp. 33–38, 2016.

[12] Y. Tomita, "Improved fracture toughness of ultrahigh strength steel through control of non-metallic inclusions," *Journal of Materials Science*, vol. 28, no. 4, pp. 853–859, 1993.

[13] J. Gao, P. Fu, H. Liu, and D. Li, "Effects of rare earth on the microstructure and impact toughness of H13 steel," *Metals*, vol. 5, no. 1, pp. 383–394, 2015.

[14] J. Pu, S. Yu, and Y. Li, "Role of inclusions in flux aided backing submerged arc welding," *Journal of Materials Processing Technology*, vol. 240, pp. 145–153, 2017.

[15] N. Yan, S. F. Yu, and Y. Chen, "Inclusions,microstructure and properties of flux copper backing submerged arc weld metal," *Science and Technology of Welding and Joining*, vol. 20, no. 5, pp. 418–424, 2015.

[16] B. Hinton, "Corrosion inhibition with rare earth metal salts," *Journal of Alloys Compounds*, vol. 180, pp. 15–25, 1992.

[17] C. Wang, F. Jiang, and F. Wang, "The characterization and corrosion resistance of cerium chemical conversion coatings for 304 stainless steel," *Corrosion Science*, vol. 46, no. 1, pp. 75–89, 2004.

[18] E. Gharibshahiyan, A. H. Raouf, N. Parvin, and M. Rahimian, "The effect of microstructure on hardness and toughness of low carbon welded steel using inert gas welding," *Materials and Corrosion*, vol. 32, no. 4, pp. 2042–2048, 2011.

[19] C. Zhang, X. Song, P. Lu, and X. Hu, "Effect of microstructure on mechanical properties in weld-repaired high strength low alloy steel," *Materials and Corrosion*, vol. 36, pp. 233–242, 2012.

[20] B. Basu and R. Raman, "Microstructural variations in a high-strength structural steel weld under isoheat input conditions," *Welding Journal (Miami, Fla)*, vol. 81, no. 11, 2002.

[21] G. Spanos, R. W. Fonda, R. A. Vandermeer, and A. Matuszeski, "Microstructural changes in HSLA-100 steel thermally cycled to simulate the heat-affected zone during welding," *Metallurgical and Materials Transactions A: Physical Metallurgy and Materials Science*, vol. 26, no. 12, pp. 3277–3293, 1995.

[22] Y. Cai, R. Liu, Y. Wei, and Z. Cheng, "Influence of Y on microstructures and mechanical properties of high strength steel weld metal," *Materials & Design (1980-2015)*, vol. 62, pp. 83–90, 2014.

[23] T. Koseki and G. Thewlis, "Inclusion assisted microstructure control in C-Mn and low alloy steel welds," *Materials Science and Technology*, vol. 21, no. 8, pp. 867–879, 2005.

[24] C. A. Williams, P. Unifantowicz, N. Baluc, G. D. W. Smith, and E. A. Marquis, "The formation and evolution of oxide particles in oxide-dispersion- strengthened ferritic steels during processing," *Acta Materialia*, vol. 61, no. 6, pp. 2219–2235, 2013.

[25] R. A. Ricks, P. R. Howell, and G. S. Barritte, "The nature of acicular ferrite in HSLA steel weld metals," *Journal of Materials Science*, vol. 17, no. 3, pp. 732–740, 1982.

[26] R. M. Fernández-Domene, E. Blasco-Tamarit, D. M. García-García, and J. García-Antón, "Effect of alloying elements on the electronic properties of thin passive films formed on carbon steel, ferritic and austenitic stainless steels in a highly concentrated LiBr solution," *Thin Solid Films*, vol. 558, pp. 252–258, 2014.

[27] Y. Chen, T. Hong, M. Gopal, and W. P. Jepson, "EIS studies of a corrosion inhibitor behavior under multiphase flow conditions," *Corrosion Science*, vol. 42, no. 6, pp. 979–990, 2000.

[28] G. A. Zhang and Y. F. Cheng, "Corrosion of X65 steel in CO_2-saturated oilfield formation water in the absence and presence of acetic acid," *Corrosion Science*, vol. 51, no. 8, pp. 1589–1595, 2009.

[29] H.-Y. Ha, M.-H. Jang, T.-H. Lee, and J. Moon, "Interpretation of the relation between ferrite fraction and pitting corrosion resistance of commercial 2205 duplex stainless steel," *Corrosion Science*, vol. 89, no. C, pp. 154–162, 2014.

[30] D. H. Kang and H. W. Lee, "Study of the correlation between pitting corrosion and the component ratio of the dual phase in duplex stainless steel welds," *Corrosion Science*, vol. 74, pp. 396–407, 2013.